CrossMark

NUMERICAL SIMULATIONS CHALLENGED ON THE PREDICTION OF MASSIVE SUBHALO ABUNDANCE IN GALAXY CLUSTERS: THE CASE OF ABELL 2142

E. Munari[1,2,3], C. Grillo[1,4], G. De Lucia[2], A. Biviano[2], M. Annunziatella[2], S. Borgani[2,3],
M. Lombardi[4], A. Mercurio[5], and P. Rosati[6]

[1] Dark Cosmology Centre, Niels Bohr Institute, University of Copenhagen, Juliane Maries Vej 30, DK-2100 Copenhagen, Denmark; munari@oats.inaf.it
[2] INAF—Osservatorio Astronomico di Trieste, via G. B. Tiepolo 11, I-34143, Trieste, Italy
[3] Dipartimento di Fisica, Università degli Studi di Trieste, via G. B. Tiepolo 11, I-34143 Trieste, Italy
[4] Dipartimento di Fisica, Università degli Studi di Milano, via Celoria 16, I-20133 Milano, Italy
[5] INAF—Osservatorio Astronomico di Capodimonte, Via Moiariello 16, I-80131 Napoli, Italy
[6] Dipartimento di Fisica e Scienze della Terra, Università degli Studi di Ferrara, Via Saragat 1, I-44122 Ferrara, Italy

ABSTRACT

In this Letter we compare the abundance of the member galaxies of a rich, nearby ($z = 0.09$) galaxy cluster, Abell 2142, with that of halos of comparable virial mass extracted from sets of state-of-the-art numerical simulations, both collisionless at different resolutions and with the inclusion of baryonic physics in the form of cooling, star formation, and feedback by active galactic nuclei. We also use two semi-analytical models to account for the presence of orphan galaxies. The photometric and spectroscopic information, taken from the Sloan Digital Sky Survey Data Release 12 database, allows us to estimate the stellar velocity dispersion of member galaxies of Abell 2142. This quantity is used as proxy for the total mass of secure cluster members and is properly compared with that of subhalos in simulations. We find that simulated halos have a statistically significant ($\gtrsim 7$ sigma confidence level) smaller amount of massive (circular velocity above $200\ \mathrm{km\ s^{-1}}$) subhalos, even before accounting for the possible incompleteness of observations. These results corroborate the findings from a recent strong lensing study of the Hubble Frontier Fields galaxy cluster MACS J0416 and suggest that the observed difference is already present at the level of dark matter (DM) subhalos and is not solved by introducing baryonic physics. A deeper understanding of this discrepancy between observations and simulations will provide valuable insights into the impact of the physical properties of DM particles and the effect of baryons on the formation and evolution of cosmological structures.

Key words: dark matter – galaxies: clusters: general – galaxies: clusters: individual (Abell 2142) – galaxies: structure – methods: numerical – methods: observational

1. INTRODUCTION

In the hierarchical structure formation scenario, galaxies form and evolve in dark matter (DM hereafter) halos that merge with other halos to assemble larger systems. Because of this process, halos are composed of a diffuse matter component and a population of subhalos, whose motion and spatial distribution are determined by dynamical processes taking place after a halo has merged into another one. Dynamical friction makes subhalos sink toward the halo center, where strong tidal fields are very effective at stripping material from the external regions of subhalos (see, e.g., Kravtsov et al. 2004; Boylan-Kolchin et al. 2008). Several other processes can act and affect the DM and baryonic components, such as tidal heating, ram-pressure-stripping, and harassment (e.g., Moran et al. 2007; Biviano 2008; Brüggen & De Lucia 2008; De Lucia et al. 2012).

In Grillo et al. (2015), the subhalo distribution inferred from the strong lensing analysis of a massive galaxy cluster, MACS J0416, is compared with the predictions of N-body simulations. This comparison shows a significant lack of massive subhalos in simulations. The latter do not include baryonic physics and this could be one of the reasons for the disagreement with the observed subhalo population. In fact, the simulated subhalos are less concentrated than they would be if they had baryons, therefore they are more fragile against tidal stripping. On the other hand, that cluster has a total density profile characterized by an inner core. This would cause tidal fields to be weaker

than in the case of a cuspy profile, such as the Navarro–Frenk–White profile (Navarro et al. 1996, 1997) found in simulated halos, leading to a larger massive subhalo population in MACS J0416 when compared with simulations.

In this paper, we analyze the subhalo distribution of a massive, nearby cluster, utilizing internal kinematics of cluster galaxies as a proxy of subhalo masses, as opposed to the strong lensing modeling techniques used in Grillo et al. (2015). We then compare the observed subhalo population with the predictions of numerical simulations.

In particular, we study Abell 2142 (A2142 hereafter), a massive ($M_{200,\mathrm{cr}} = (1.25 \pm 0.13) \times 10^{15} M_{\odot}$) cluster at $z \sim 0.09$ (Munari et al. 2014, M14 hereafter). The cluster was studied by several authors using different probes, namely X-ray (Markevitch et al. 2000; Akamatsu et al. 2011; Rossetti et al. 2013), the Sunyaev-Zel'dovich effect (Umetsu et al. 2009), weak lensing (Okabe & Umetsu 2008), and galaxy dynamics (Owers et al. 2011, O11 hereafter; M14), and although it possesses several subclumps in the galaxy distribution (O11), these do not appear to affect the dynamical equilibrium of the cluster significantly (M14).

2. THE DATA SET

2.1. The Observations

Based on the spectroscopic catalog provided by O11, here we use the membership of A2142 that was computed by M14. We restrict our analysis to the inner 2.2 Mpc in projection,

which is very close to the virial radius of A2142 found by M14, and, as done in that study, adopt the X-ray center provided by De Grandi & Molendi (2002) as the cluster center. The number of galaxy members extracted from the O11 catalog is $N_{mem} = 721$ within 2.2 Mpc from the cluster center. The analysis by O11 has a magnitude limit of 20.5 in the R band of the Johnson–Cousins system (R_{JC} hereafter). We anticipate that this limit corresponds to values of circular velocity that are well below those that we probe in this work, thus not affecting our main results.

We use the photometric information contained in the Sloan Digital Sky Survey Data Release 12 (SDSS DR12) database[7], selecting galaxies with $238°.983 <$ R.A. $<$ $240°.183, 26°.633 <$ decl. $< 27°.834$, and petroMag$_r < 25$. This magnitude limit ensures that we include all the members. We match this catalog with the member catalog by requiring objects to be closer than 0.06 arcsec ($\simeq 6$ kpc at the cluster redshift) in projection. The number of cluster members with SDSS photometric information is $N_{mem \cap ph} = 708$, within 2.2 Mpc from the cluster center.

Then we extract from the SDSS DR12 spectroscopic sample the galaxies that satisfy the same criteria used for the photometric selection, further requiring only objects with secure redshifts, and retrieve $N_{sp} = 288$ galaxies within 2.2 Mpc from the cluster center. For these objects, we estimate aperture-corrected stellar velocity dispersion values σ_0, i.e., the velocity dispersion of stars within an eighth of the galaxy effective radius, following the prescription presented in Jorgensen et al. (1995), and using the SDSS values of the galaxy effective radii $R_{e,i}$ in the i band. We perform the matching of this catalog with that of cluster members by imposing the same limit in projected distance as before and a relative difference in redshift smaller than 1%. The matched cluster galaxies are $N_{mem \cap sp} = 187$.

We further restrict our analysis to elliptical galaxies by considering only objects with fracDev_i > 0.8. This quantity is the best fitting coefficient of the de Vaucouleurs term obtained from the decomposition of the surface brightness profile in the i band of each galaxy in terms of a linear combination of exponential and de Vaucouleurs profiles. This photometric criterion ensures that the selected objects are very likely elliptical galaxies (see also Grillo 2010). The number of elliptical members is $N_{mem \cap sp,E} = 146$.

According to the same criterion, we also select elliptical galaxies from the photometric catalog, with the further requirement that $R_{e,i} > 0.3$ kpc, to exclude galaxies with unreliable effective radii. This results in $N_{mem \cap ph,E} = 324$ galaxies within 2.2 Mpc from the cluster center.

2.2. The Simulations

Here we briefly summarize the main features of the simulations used for this work and we refer the reader to Rasia et al. (2015) for a more detailed description. Starting from a low-resolution DM-only simulation, 29 massive clusters are identified and resimulated at higher resolution with the zoom-in technique, with different implementations for baryonic physics. The low-resolution parent simulation consists of 1024^3 particles in a 1 h^{-1} Gpc box, realized with the GADGET 3 code, an improved version of the GADGET 2 code (Springel 2005). A flat ΛCDM cosmology with $\Omega_m = 0.24$, $\Omega_{bar} = 0.04$,

$H_0 = 72$ km s^{-1} Mpc^{-1}, $n_s = 0.96$, and $\sigma_8 = 0.8$ is adopted. In this work we use four sets of such simulations, with two different implementations of baryonic physics. The "DMHR" is a collisionless realization with a particle mass of $m_{DM} = 1 \times 10^8$ h^{-1} $M_\odot$ and a Plummer-equivalent softening length of $\epsilon = 2.5$ h^{-1} kpc in physical units below $z = 2$ (fixed in comoving units at higher redshift). The "DMLR" is a lower-resolution version of the DMHR, with $m_{DM} = 1 \times 10^9$ h^{-1} $M_\odot$ and $\epsilon = 5$ h^{-1} kpc. The "CSF" set implements a metallicity-dependent radiative cooling and a sub-resolution model for star formation with Chabrier IMF (Chabrier 2003). A uniform time-dependent UV background is included, while kinetic feedback contributed by supernovae is implemented in the form of winds with a velocity of ~ 350 km s^{-1}. Metal production and ejection into the inter-stellar medium are modeled as in Tornatore et al. (2007). The "AGN" set implements the additional effect of active galactic nuclei feedback, modeled following Steinborn et al. (2015). The two sets with baryon physics have the same DM particle mass and force resolution as the DMLR set. The algorithm SUBFIND (Springel et al. 2001; Dolag et al. 2009) is used to separate the subhalos from the diffuse matter of the cluster halo, by searching overdensities of bound DM and star (in the hydrodynamical runs) particles in the cluster density field.

The baryonic component of a subhalo, i.e., a galaxy, is usually more compact than the subhalo, and is therefore more resistant against the stripping due to cluster tidal fields. The external part of a subhalo can eventually be entirely stripped, leaving only the galaxy. Such galaxies that have lost their DM envelope are called "orphans." N-body simulations, lacking the compact baryonic cores, are not able to reproduce the population of orphan galaxies. On the contrary, hydrodynamical simulations have the compact baryonic cores, but due to resolution limitations, they might not capture the whole population of orphan galaxies. For this reason, we also use two different semi-analytical models, namely those described in De Lucia & Blaizot (2007, hereafter DLB07) and Henriques et al. (2015, hereafter HEN15), to which we refer for further details. Both these models use subhalo merger trees extracted from high-resolution N-body simulations (the "Millennium" simulation (Springel 2005), on which subhalos are identified using SUBFIND as in the hydrodynamical simulations described above) as input. When a subhalo is stripped below the resolution of the simulation, the galaxy it hosts becomes an "orphan" galaxy and is assigned a residual merger time based on variations of the classical Chandrasekhar formula (Chandrasekhar 1943). The two models differ for the specific prescriptions adopted to describe various physical processes, and predict different amounts of orphan galaxies in clusters.

We select galaxy clusters with virial masses values larger than 10^{15} $M_\odot$ at the redshift closest to that of A2142, namely $z = 0$ for DMHR and DMLR, $z = 0.1$ for CSF and AGN, $z = 0.09$ for DLB07, and $z = 0.08$ for HEN15. In this way we select galaxy clusters with virial masses comparable to that of A2142, namely $1.25 \times 10^{15} M_\odot$ (M14). We simulate the line-of-sight effects of observations by projecting each cluster along three orthogonal directions. The selected samples consist of 22, 25, 22, 21, 18, 23 clusters, observed in 3 directions, for a total of 66, 75, 66, 63, 54, 69 systems in projection in the DMHR, DMLR, CSF, AGN, DLB07, HEN15 sets, respectively. We consider the two-dimensional (2D) distance of each subhalo from the cluster center, selecting those within 2 virial radii

along the direction of projection, in order to include objects residing in the cluster outskirts, but excluding interlopers. For all subhalos, we store the values of circular velocity v_c, defined as the maximum value of $\sqrt{G\,M(<r)/r}$, $M(<r)$ being the mass within the three-dimensional (3D) distance r from the center of the subhalo. For the orphan galaxies in the semi-analytic models, the adopted circular velocity is the value the subhalo had at the last snapshot before disappearing below the resolution limit.
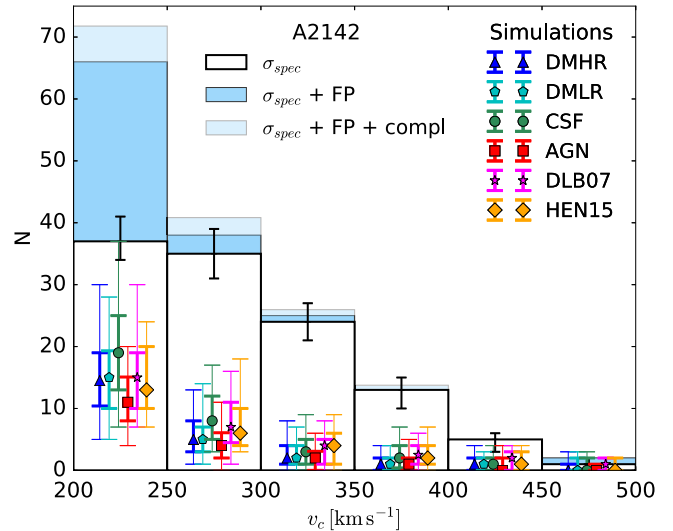
3. CIRCULAR VELOCITY DISTRIBUTION

Several observational and theoretical studies have shown that in massive early-type galaxies (ETGs) the DM and stellar components combine to produce a total mass density profile that can be well-approximated by an isothermal profile, although neither of the two components have precisely such a profile. This is the so-called "bulge-halo conspiracy." ETGs from the SLACS survey were studied by Auger et al. (2010), combining different probes, and by Barnabè et al. (2011) combining stellar kinematics and gravitational lensing, while Cappellari et al. (2015) applied dynamical models on a sample of 14 fast rotators ETGs out to a median radius of $\sim 4\,R_e$ (~ 10 kpc). All these studies found that an isothermal profile is a good description of the galaxy total mass density profile. Using the *Chandra X-ray Observatory*, Humphrey & Buote (2010) studied a sample of objects spanning ~ 2 orders of magnitude in mass, from ETGs to galaxy clusters. They concluded that an isothermal profile is a good description of the total mass profile of galaxies out to $\sim 10\,R_e$, where DM dominates the mass budget. Gavazzi et al. (2007) performed a joint strong and weak lensing analysis of 22 massive ETGs, finding that the lenses are described well by an isothermal profile out to $\sim 100\,R_e$ (few hundreds kpc), with an effective velocity dispersion value very similar to that of the central stellar velocity dispersion.

On the theoretical side, Dutton & Treu (2014) constructed ΛCDM-based mass models to reproduce the observed structural and dynamical scaling relations of ETGs in the SDSS and showed that all models produce roughly isothermal total mass density profiles. By studying 35 simulated spheroidal galaxies, Remus et al. (2013) concluded that the isothermal profile, resulting from the combination of the stellar and DM components, acts as an attractor solution of the complex dynamics of the system (although this mechanism has still unclear explanations).

In the innermost regions of ETGs, stars dominate the total mass budget, so here their velocity dispersion σ_0 is representative of the velocity dispersion of the whole system, as shown, e.g., in Saglia et al. (1992) and Thomas et al. (2007). Treu et al. (2006) and Grillo et al. (2008) have found that σ_0 is, within the uncertainties, equal to σ_{1D}, which is the parameter that characterizes an isothermal profile. On the other hand, in simulations it is straightforward to measure the circular velocity of a subhalo, v_c, as explained in Section 2.2.

For a generic system, the one-dimensional velocity dispersion σ and circular velocity v_c are related as follows: $v_c = \sigma \times \sqrt{\gamma}$ where $\gamma = -d\ln\rho/d\ln r$ is the logarithmic derivative of the mass density. If we assume that the stellar mass density profile of ETGs is well described by their luminosity distribution, and use the Jaffe model (Jaffe 1983) for it, we obtain $\gamma = 2$ at $r = 0$, and $\gamma = 4$ at large r. Hereafter we use $\gamma = 2$; using $\gamma > 2$ would only strengthen our

Figure 1. Distribution of the values of circular velocity of member galaxies within 2.2 Mpc in projection from the cluster center. The white histogram refers to the sample of A2142 members with measured velocity dispersion from the SDSS DR12 spectroscopic sample (mem ∩ sp, E). The histogram with error bars represents the median value, with its 16th and 84th percentiles, in each bin (see the text for details). The blue histogram extends the distribution to members that have velocity dispersions estimated from the Fundamental Plane. When the sample completeness is considered, the pale blue histogram is obtained. The symbols with error bars are the median values of circular velocity of subhalos in different simulated clusters, as indicated in the legend. Thick and thin error bars indicate the 16th–84th percentiles and the minimum–maximum values, respectively.

conclusions (see below). A conversion factor close to $\sqrt{2}$ or slightly higher is reported in Cappellari et al. (2013), who performed a detailed axisymmetric dynamical modeling of a large sample of observed ETGs. In the following, the values of velocity dispersion will be converted into circular velocity values to compare observations against simulations.

In Figure 1, we show the distribution of values of circular velocity of A2142 member elliptical galaxies, within 2.2 Mpc from the cluster center. The white histogram refers to the sample of elliptical cluster members with measured velocity dispersion from the SDSS spectroscopic sample (mem ∩ sp, E). To account for the errors on the measurement of the velocity dispersion, we consider 10,000 realizations of the sample, where the value of the velocity dispersion of each galaxy is taken from a normal distribution having mean and standard deviation values that are equal, respectively, to those of the aperture-corrected SDSS central stellar velocity dispersion and its error. The histogram shows the median value in each bin, and the error bars represent the 16th and 84th percentiles.

Then, we use the elliptical cluster members that have measured values of velocity dispersion σ_0 (mem ∩ sp, E) to calibrate the Fundamental Plane and estimate the velocity dispersion values of the elliptical cluster members that do not have SDSS spectroscopic information. The Fundamental Plane is a scaling law (see, e.g., Djorgovski & Davis 1987; Dressler et al. 1987; Bernardi et al. 2003 and references therein) that relates the values of effective radius, central stellar velocity dispersion, and surface brightness SB_e within the effective radius of elliptical galaxies:

$$\mathrm{Log}(\sigma_0) = \alpha + \beta \times \mathrm{Log}(R_e) - \gamma \times SB_e. \tag{1}$$
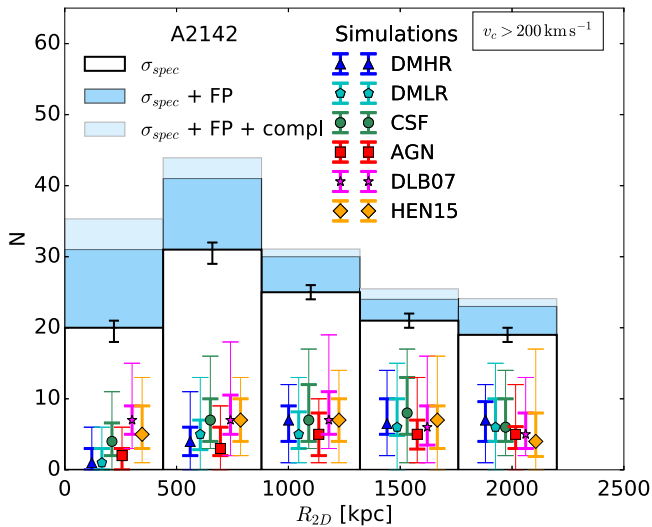
Figure 2. Projected radial distributions of the galaxies shown in Figure 1, with the same color-coding. The analysis is restricted to the galaxies having circular velocity values larger than 200 km s^{-1}.

We restrict our analysis to the galaxies with velocity dispersion above 90 km s^{-1} and find the following values: $\alpha = 6.84 \pm 0.26$, $\beta = 0.64 \pm 0.04$, $\gamma = 0.24 \pm 0.01$. From this relation, we get an estimate of the velocity dispersion of the elliptical members for which a spectroscopic measurement is not available. The blue histogram of Figure 1 shows the distribution of the values of circular velocity of the members that have either a spectroscopic measurement of velocity dispersion or a velocity dispersion estimate inferred from the Fundamental Plane, as explained above. When this last histogram is corrected to account for the incompleteness of the sample, we obtain the pale blue histogram. We here provide an approximate estimate of the completeness. O11 provide an estimate of the completeness of their spectroscopic catalog by comparing it with their photometric catalog (see their Figure 2). We use their estimate as completeness C_M. We consider both the radial and the magnitude dependence of C_M. Since O11 use the Johnson–Cousins R system, we convert the g and r SDSS bands into that system to account for the magnitude dependence of C_M. To each galaxy in the sample of member elliptical galaxies (mem ∩ ph, E), we assign a weight equal to C_M^{-1}, according to the galaxy projected distance from the cluster center and magnitude. In this way, we compute the completeness-corrected distributions.

The symbols with error bars in Figure 1 are the median values for the simulated clusters, with thick and thin error bars indicating the 16th–84th percentiles and minimum–maximum values, respectively. We notice that the low-resolution and high-resolution DM-only simulations provide a comparable amount of subhalos, indicating that for massive subhalos resolution is not affecting the results, and the different estimates provided by the CSF and AGN sets are due to the inclusion of baryonic physics. We verified that the number of subhalos with circular velocity below the values probed in our analysis is enhanced in the hydrodynamical runs.

The semi-analytic models predict an amount of massive subhalos similar to that of N-body and hydrodynamical simulations, suggesting that orphan galaxies do not contribute

considerably to the population of subhalos at the high-mass end.

For circular velocities in the range 200–400 km s^{-1}, we find a statistically significant difference between the values of measured velocity of cluster members in A2142 and those of simulated subhalos. Simulated clusters present fewer subhalos, with a discrepancy that is at $\gtrsim 7$ sigma significance level (13.0, 11.9, 6.9, 12.7, 11.6, 10.0 significance level for, respectively, DMHR, DMLR, CSF, AGN, DLB07 and HEN15 sets. These values become 11.3, 10.0, 7.6, 12.3, 9.5, 8.8 when restricting the analysis to the inner 1 Mpc). We remark that this result is robust, as we are comparing the outcomes of simulations and direct measurements of velocities, without any intermediate mass calibration (as done for strong lensing analyses). The result is even more striking if one considers that it is just a lower limit. In fact the members with spectroscopic velocity dispersions are just a fraction of the entire population of galaxy members. This is shown by the other two histograms that include an estimate of the circular velocity of elliptical members that have no SDSS spectroscopic information and then also take into account the completeness of the sample. The discrepancy is exacerbated by the fact that we only consider ETGs in A2142, while we consider the whole population of subhalos in simulated clusters.

Finally, we check whether the missing simulated subhalos are preferentially located at some particular distance from the cluster center. In Figure 2, we plot the radial distribution of the galaxies shown in Figure 1, restricting our analysis to galaxies with circular velocity values larger than 200 km s^{-1}. Our results do not depend on the distance from the cluster center.

To check the robustness of our results, we fit the magnitude-circular velocity relation and find that the adopted magnitude limit $R_{JC} > 20.5$ of O11 corresponds to a circular velocity of approximately 20 km s^{-1}, well below the lower limit of 200 km s^{-1} used in our analysis.

4. CONCLUSIONS

Our analysis indicates that current numerical simulations predict a significant smaller amount of massive (circular velocity above 200 km s^{-1}) subhalos. This result is robust, as it holds even when we compare the predictions of simulations and the direct measurements of velocity values of cluster members, without addressing incompleteness issues. When accounting for the latter, the actual number of observed galaxies becomes larger, making the discrepancy even more significant. These results support the findings of a recent strong lensing study of the Hubble Frontier Fields galaxy cluster MACS J0416 at $z = 0.4$ (Grillo et al. 2015), suggesting that this discrepancy, which is already present in DM-only simulations, is not alleviated by the inclusion of baryonic physics.

REFERENCES

Akamatsu, H., Hoshino, A., Ishisaki, Y., et al. 2011, PASJ, 63, S1019
Auger, M. W., Treu, T., Bolton, A. S., et al. 2010, ApJ, 724, 511
Barnabè, M., Czoske, O., Koopmans, L. V. E., Treu, T., & Bolton, A. S. 2011, MNRAS, 415, 2215
Bernardi, M., Sheth, R. K., Annis, J., et al. 2003, AJ, 125, 1866
Biviano, A. 2008, arXiv:0811.3535
Boylan-Kolchin, M., Ma, C.-P., & Quataert, E. 2008, MNRAS, 383, 93
Brüggen, M., & De Lucia, G. 2008, MNRAS, 383, 1336
Cappellari, M., Romanowsky, A. J., Brodie, J. P., et al. 2015, ApJL, 804, L21
Cappellari, M., Scott, N., Alatalo, K., et al. 2013, MNRAS, 432, 1709
Chabrier, G. 2003, PASP, 115, 763
Chandrasekhar, S. 1943, ApJ, 97, 255
De Grandi, S., & Molendi, S. 2002, ApJ, 567, 163
De Lucia, G., & Blaizot, J. 2007, MNRAS, 375, 2
De Lucia, G., Weinmann, S., Poggianti, B. M., Aragón-Salamanca, A., & Zaritsky, D. 2012, MNRAS, 423, 1277
Djorgovski, S., & Davis, M. 1987, ApJ, 313, 59
Dolag, K., Borgani, S., Murante, G., & Springel, V. 2009, MNRAS, 399, 497
Dressler, A., Lynden-Bell, D., Burstein, D., et al. 1987, ApJ, 313, 42
Dutton, A. A., & Treu, T. 2014, MNRAS, 438, 3594
Gavazzi, R., Treu, T., Rhodes, J. D., et al. 2007, ApJ, 667, 176
Grillo, C. 2010, ApJ, 722, 779
Grillo, C., Lombardi, M., & Bertin, G. 2008, A&A, 477, 397
Grillo, C., Suyu, S. H., Rosati, P., et al. 2015, ApJ, 800, 38

Henriques, B. M. B., White, S. D. M., Thomas, P. A., et al. 2015, MNRAS, 451, 2663
Humphrey, P. J., & Buote, D. A. 2010, MNRAS, 403, 2143
Jaffe, W. 1983, MNRAS, 202, 995
Jorgensen, I., Franx, M., & Kjaergaard, P. 1995, MNRAS, 276, 1341
Kravtsov, A. V., Gnedin, O. Y., & Klypin, A. A. 2004, ApJ, 609, 482
Markevitch, M., Ponman, T. J., Nulsen, P. E. J., et al. 2000, ApJ, 541, 542
Moran, S. M., Ellis, R. S., Treu, T., et al. 2007, ApJ, 671, 1503
Munari, E., Biviano, A., & Mamon, G. A. 2014, A&A, 566, A68
Navarro, J. F., Frenk, C. S., & White, S. D. M. 1996, ApJ, 462, 563
Navarro, J. F., Frenk, C. S., & White, S. D. M. 1997, ApJ, 490, 493
Okabe, N., & Umetsu, K. 2008, PASJ, 60, 345
Owers, M. S., Nulsen, P. E. J., & Couch, W. J. 2011, ApJ, 741, 122
Rasia, E., Borgani, S., Murante, G., et al. 2015, ApJL, 813, L17
Remus, R.-S., Burkert, A., Dolag, K., et al. 2013, ApJ, 766, 71
Rossetti, M., Eckert, D., De Grandi, S., et al. 2013, A&A, 556, A44
Saglia, R. P., Bertin, G., & Stiavelli, M. 1992, ApJ, 384, 433
Springel, V. 2005, MNRAS, 364, 1105
Springel, V., Yoshida, N., & White, S. D. M. 2001, NewA, 6, 79
Steinborn, L. K., Dolag, K., Hirschmann, M., Prieto, M. A., & Remus, R.-S. 2015, MNRAS, 448, 1504
Thomas, J., Saglia, R. P., Bender, R., et al. 2007, MNRAS, 382, 657
Tornatore, L., Borgani, S., Dolag, K., & Matteucci, F. 2007, MNRAS, 382, 1050
Treu, T., Koopmans, L. V., Bolton, A. S., Burles, S., & Moustakas, L. A. 2006, ApJ, 640, 662
Umetsu, K., Birkinshaw, M., Liu, G.-C., et al. 2009, ApJ, 694, 1643